Iranian Journal of Geophysics, Vol 16 No 4, 2023, Page 193 – 209 (Research Article)
DOI:10.30499/IJG.2023.350802.1442

Structural deformation analysis of parts of Nigeria's southwestern precambrian basement complex using gradient techniques

Kesyton Oyamenda Ozegin[1*] and Owens Monday Alile[2]

[1] *Ph.D. in Exploration Geophysics, Department of Physics, Ambrose Alli University, Ekpoma Edo State, Nigeria*
[2]*Professor, Department of Physics, University of Benin, Benin City, Nigeria*

(Received: 8 July 2022, Accepted: 5 January 2023)

Abstract

A distinctive attribute of basement complex terrain is the widespread manifestation of structural deformations. Locating these structural deformations, such as faults, fractures, folds, and joints of the basement complex terrain, is a preface to hydrogeologic, engineering, and environmental studies as well as mineral resource exploration programs. The present study aims to delineate the subsurface structures and establish geometry and depths of magnetic anomalies in the region of Igarra Schist Belt of parts of the Southwestern Precambrian Basement Complex of Nigeria using gradient (Euler deconvolution and filtering) techniques. The 3D Euler approach estimates the location of a simple entity using magnetic field measurements by splitting the data into windows of subsequent measurements. Based on its structural index, each window calculates a single average depth and magnetic source position, while filtering is essentially employed to delineate subsurface geologic features using standard deviation. To filter data, the standard deviation filter returns the data's local distribution, with the magnitude of the effect depending on the feature's quantity. The finding showed lots of these geological features (± 95%) are located at shallow depths 0f 0 - 300 m and few are located at depths >300 m. The research region's combined data was used to generate a consistent structural map that depicted the likely placements and trends of the putatively fractured/faulted zone, as well as additional basement structures that formed in tetra-modal NE-SW, ESE-WNW, ENE-WSW, and E-W directions. These structural tendencies, which vary in intensity and length, are sturdily related to tectonic activities and over and above guidance for geoelectric studies required for hydrogeologic and engineering explorations.

Keywords: Schist Belt, structural features, magnetic anomalies, geologic contacts, exploration

*Corresponding author: ozeginkess@yahoo.com

1 Introduction

Structural features or deformations such as faults, folds, fractures, and joints (potential field anomalies) are commonplace in basement complexes, the importance of which cannot be overemphasized. This is because locating the depth and geometry of such structures serves as a possible host or passage conduit when exploring hydrocarbons, mineral resources, and groundwater (Okpoli and Eyitoyo 2016; Ozegin and Alile, 2021). Disparities between recorded magnetic values and expected results from a model of the Earth's core field are known as anomalies in the magnetic field of the Earth (U.S. Geological Survey 1997). When magnetic anomalies are discovered over sedimentary terrain, they are frequently caused by underlying basement (igneous and/or metamorphic) rocks or igneous structures such as intrusive plugs, dykes, sills, lava flows, and volcanic centers (Gunn 1997).

Airborne magnetic or aeromagnetic surveys were developed after it was discovered that the strongest magnetic anomalies formed around the surface of the basement complex and that the wavelengths of these anomalies grew as the basement rocks sank deeper. Techniques were developed to determine the depths of magnetic sources and, as a result, the thickness of the sedimentary basins covering them. Airborne magnetic investigations or surveys use a non-destructive technique that determines the susceptibility contrast of subsurface rocks. This method stands out most when compared to other geophysical methods because of its quick rate of coverage and affordable price per unit area studied (Reford and Sumner 1964). The adoption of this technology allows geophysicists and geologists to collect data regardless of who owns or has access to remote territories of interest. Because of this inherent advantage, large-scale aerial magnetic surveys have become possible all over the world. Faults, shear zones, and fractures have been located using large-scale aerial magnetic surveys (Okpoli 2019). Such zones, according to Paterson and Reeves (1985), could be prospective hosts for a variety of minerals as well as a guide for researching environmental and strain mineralization in the bedrock.

The lateral changes in the earth's magnetic field are generally reflected in aerial magnetic anomaly maps (Burger et al. 2006). Changes in structure, magnetic susceptibility, and remanent magnetization are all factors that influence these variations. Magnetic data filtering is a preface to magnetic data interpretation. It involves a wide range of transformations of the processed data that assist in its ultimate interpretation. These usually involve the application of mathematical filters or models. The acquired airborne magnetic data are usually in the form of maps, and these permit the application of quantitative interpretations to find the geometry and depth of magnetic sources. As a result, aeromagnetic surveys can be used to map geologic structure on or within basement rocks (igneous and/or metamorphic) or to directly discover magnetic minerals that reflect lateral fluctuations in the earth's magnetic field (Burger et al. 2006; Ozegin and Alile, 2021). Aeromagnetic surveys with finer line spacing, according to Nabighian et al. (2005), will reveal Intrasedimentary lithology, mineralized faults, and geochemical change in reconnaissance zones.

The significant improvements made in geophysical techniques in recent years led to regular gathering of potential fields' datasets for analysis and reliability. One of the ways of analyzing potential field data quantitatively is through the application of the Euler deconvolution technique. Thompson (1982) was the first to use the Euler deconvolution technique to profile data, progressed by Reid et al. (1990), for gridded data. Automatic interpretation techniques like Euler deconvolution can help with the quantitative interpretation of massive volumes of data gathered from the survey (Derrheim and Cooper 1997).

Hence, this technique is used to estimate the depth and geometry of structural features for homogeneous functions. In the studies of Mushayandebvu et al. (2004), Euler deconvolution is a well-known interpretation method for detecting the source location of possible field anomalies. Because it requires no prior information about the magnetic source geometry and, more importantly, no knowledge of the magnetization vector, Euler deconvolution is widely employed in magnetic interpretation (Thompson 1982; Reid et al. 1990). Higher derivatives of the interpreted field and a structural index (SI or N) linked to the homogeneity degree of the source defining potential field functions are used in the Euler deconvolution approach. A widespread solution for source positions has indeed been proven to be caused by a poor choice of structural index. Fourier transformations are very helpful for converting from the frequency response to the wavenumber domain as well as calculating derivatives (Telford et al. 1990). On the contrary, some enhancement processes can distort data; therefore, care should be taken to ensure upgraded data is used appropriately. In this paper, we attempt to estimate the depth and geometry of the magnetic body in the study area using high-resolution aeromagnetic data, which will provide valuable information on structural features or deformations in the area. The integration of Euler deconvolution and filtering techniques is used in this research. These gradient algorithms have the advantage of only requiring a few hypotheses to provide source location information.

1.1 Study area

Longitudes 6°00 and 6°30E, as well as latitudes 7°00 and 7°30N, define the study area (Figure 1). A network of highways and well-developed pathways provide access to the area. Nigeria is in the late Precambrian to early Paleozoic orogenesis zone, as is the remainder of the West African Craton. Nigeria's crystalline rocks are made up of Precambrian basement complexes and Phanerozoic rocks. Throughout geological time, these crystalline basement rocks have been subjected to various degrees of deformation.

This research area's geological map is part of Nigeria's Precambrian Southwestern Basement Complex. Proterozoic complex rocks are composed of older and younger granites, as well as younger and older tertiary and secondary sedimentary rocks. This area covered about 40% of the landmass of Nigeria and underlain by basement rocks (Obaje 2009). Metamorphic rocks such as schist and gneiss make up the majority of the Precambrian basement (Peterson 1985). The Archean to early Palaeozoic metamorphic rock complex (2,700-2,000 Ma) is contained within these rocks. Other units include NE-SW trending schist belts, which are predominantly found in the western half of the country, and granitoid plutons from the Late Proterozoic to early Phanerozoic Older Granite Suite (750 to 450 Ma). Amphibolites, Migmatite gneisses, granites, and pegmatites are the primary lithologies of the Southwestern Nigeria basement complex. The biotite, quartzite, tremolite, and muscovite schists are among the others. These schistose rocks were intruded by crystalline rocks (Oyinloye 2011).

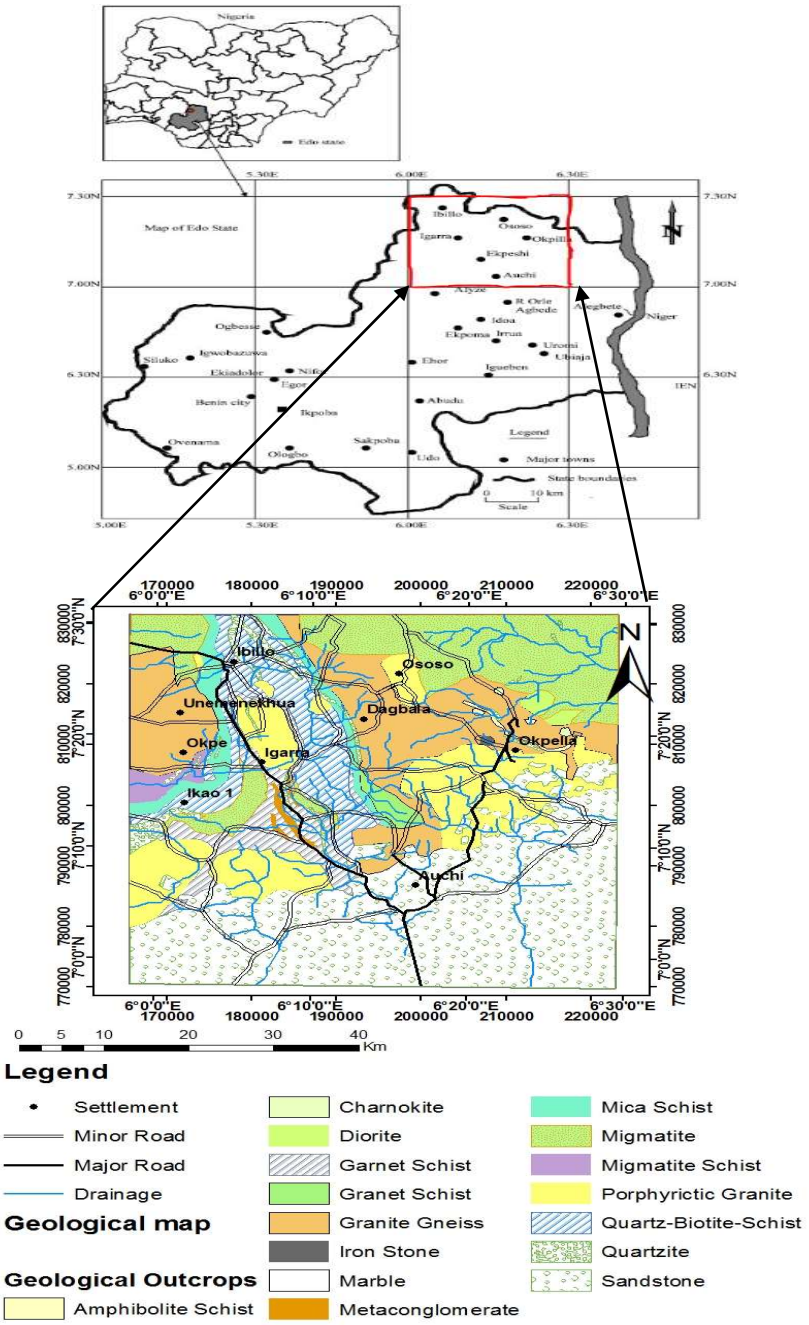

Figure 1. Map of the study area (inserts; maps of Nigeria and Edo State with a simplified geologic map of the study area (modified after Anifowose et al. 2006)).

2 Methodology

The Nigerian Geological Survey Agency (NGSA) provided the total-field, high-resolution digital airborne magnetic data used in this investigation. After the measurements were corrected for temporal changes in the magnetic field, the total magnetic intensity (TMI) anomaly was computed by subtracting the theoretical geomagnetic field or IGRF (International Geomagnetic Reference Field) at each station. The processed TMI decreased to the equator and continued upward to 100 meters over the study region. The data was inverted for different geophysical models as well as for structures using the Geosoft

Oasis MontajTM version 6.4.2 (HJ) software package to determine the source of the anomalies found in the reduced magnet data. Pictures with two-dimensional Fast Fourier Transformation (2D-FFT) filters were displayed using the grids and image tools.

By subtracting the regional field impact from TMI data, the first-order residual magnetic anomaly (RMA) was obtained, which was then improved using a variety of techniques (Figure 2). Reduction to the equator (RTE), vertical derivative (VD), and total horizontal derivative (THD) are among the signal improvement techniques used for qualitative interpretation.

The RTE was employed to remove the asymmetry and declination effects in order to maintain a low angle of inclination at the equator, resulting in a horizontal source of magnetization. The RTE map aims to minimize magnetic declination impact in the negative magnetic latitude zone by centering magnetic anomalies over their sources and augmenting the basement architecture, incorporating structural lineaments with their orientations (Ndougsa-Mbarga 2012; Owono 2019; Ozegin and Alile 2021).

The VD was used to obtain total magnetic intensity data to improve the characterization of source body borders and highlight shallow geologic sources. VD maps are more susceptible to local effects than regional or broad effects, and hence provide a clearer image than TMI maps. The algorithm is given by (Gunn1997; Hani et al. 2013) as:

$$A(u,v) = [(u2 + v2)0.5/n]n \quad (1)$$

where n is the order of the derivative, and A (u, v) represents the amplitude existing at those frequencies.

Because the map becomes noisier as the order of derivatives increases, the first order was chosen.

The total horizontal derivative filter is a useful tool for locating geologic connections between bodies in the soil, and it emphasizes shallow anomalies. THD has the advantage of being impervious to noise introduced by data collected during an aeromagnetic survey, as it relies solely on the calculation of the magnetic field's major derivatives in the horizontal map (Phillips 1998; Owono 2019). As a result, the structural characteristics and bounds of causal sources can be improved.

To estimate the positions and depths of the source of magnetic anomalies in the area, the Euler deconvolution, a quantitative interpretation of airborne magnetic data, was used. The quantitative interpretation of magnetic anomalies is to find a source distribution whose anomalous field fits the actual field on the measuring surface as closely as possible. The solution was found by inverting the Euler homogeneity equation, which links the magnetic field and its gradient components to the source location of an anomaly and the degree of homogeneity expressed as a structural index. The structural index, N, is the most crucial parameter in the Euler deconvolution (Thompson 1982). The structural index is a measurement of a field's rate of change in its distance (John and Emmanuel 2014). Poor N selection has been proven to result in widespread resolution of source locations and significant depth estimation problems (Moghaddam et al. 2015; Olawuyi 2018; Okwesili et al. 2019). Thompson (1982) and Reid et al. (1990) claim that a correct N results in the closest cluster formation of Euler solutions around the geologic feature of concern. For this study, a structural index of 0.0 gives the tightest clustering. The structural trends were integrated into the ArcGIS 10.5 software environment, georeferenced, and digitized to provide structural trends that were utilized to characterize the linear characteristics in the research area, and a rose diagram was generated using Georient software.

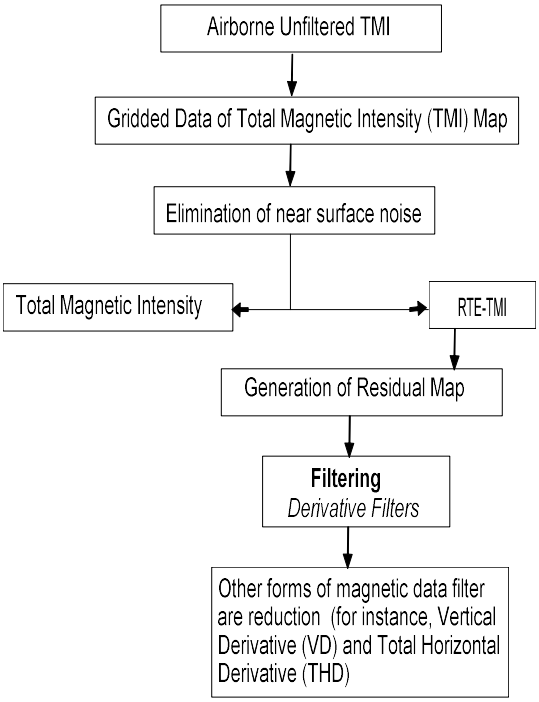

Fig 2. A simplified flow chart for data processing and interpretation

2.1 Theory of Euler deconvolution

Over the years, geophysicists and geologists have been fascinated by Euler's homogeneity relation. Thompson (1982) proposed the Euler deconvolution hypothesis as follows:

Any degree n function $f\ (x,\ y,\ z)$ is homogenous if:

$$f\ (tx,\ ty,\ tz)=t^n f\ (x,\ y,\ z), \qquad (2)$$

where t is an even number. The observation plane starts at z = 0 and descends with positive z. Furthermore, the following equation applies if $f\ (x,\ y,\ z)$ is homogeneous of degree n.

$$x\frac{\partial f}{\partial x}\ +\ y\frac{\partial f}{\partial y}\ +\ z\frac{\partial f}{\partial z}\ =\ nf \qquad ..(3)$$

Euler's homogeneity equation is, of course, the name of this partial differential equation. The total magnetic intensity of a point source placed at a location in reference to the observation point is as follows:

$$T(x,\ y)\ =\ f[(x\ -\ x_0),\ (y\ -\ y_0),\ (z\ -\ z_0)] \qquad (4)$$

With a measurement point at $(x,\ y,\ z)$, we calculate the overall magnetic field variance over such a simple structure and a body center at $(x_0,\ y_0,\ z_0)$ in this research. Euler's equation can thus be expressed as:

$$(x\ -\ x_o)\frac{\partial T}{\partial x}\ +\ (y\ -\ y_o)\frac{\partial T}{\partial y}\ +\ (z\ -\ z_o)\frac{\partial T}{\partial z}\ =\ N(B\ -\ T) \qquad (5)$$

Where $(x_0,\ y_0,\ z_0)$ denotes the location of a source whose total field T is visible at $(x,\ y,\ z)$. B is the regional or background number for the entire field. The N parameter's value is determined by the kind of geologic source body, which includes faults, contacts, dykes, cylinders, and spheres. For the N parameter, the following values for magnetic sources and simple models are valid (Table 1).

Table 1 Simple models and structural indexes for magnetic sources

Magnetic source and simple model	Structural Index (N)
Contact; Infinite sheet	0
Line of poles; dike; sill	1
Point pole; Line of dipoles; horizontal or vertical cylinder	2
Point dipole; sphere	3

Source: (Thompson 1982 and Florio et al. 2006)

3 Results and Discussion

3.1 Total airborne magnetic intensity map

The Total magnetic intensity (TMI) map (Figure 3) in the study area showed anomalies characterized by areas that are susceptible to high magnetic in low magnetic values and vice versa suggestive of distinct rock types in the area. It basically makes valuable as well as striking information for the description of vital geologic features of the subsurface available. Total magnetic intensity values in the study area ranged from -104.1 (minimum) to 71.2 nT (maximum), with an average value of 3.29 nT, symptomatic of differing magnetic propensities or mineral composition differences in the research area's rock types. It shows that the relatively high magnetic intensity values between 1.6 and 71.2 nT correspond largely to sandstone, Migmatite, and granite gneiss on the geological map of the study area (Figure 1). In the same manner, the moderately low magnetic intensity values between −5.2 and −104.1 nT are notably found on Garnet schist and porphyritic granite. These low anomalies most likely represent reasonably magnetic bedrock with nonmagnetic material within the fracture or depressed zone, which may be sand, clay, or chemically produced sediment. The overall field intensity map had previously been adjusted for the area's highly variable main earth magnetic and temporal diurnal fields.

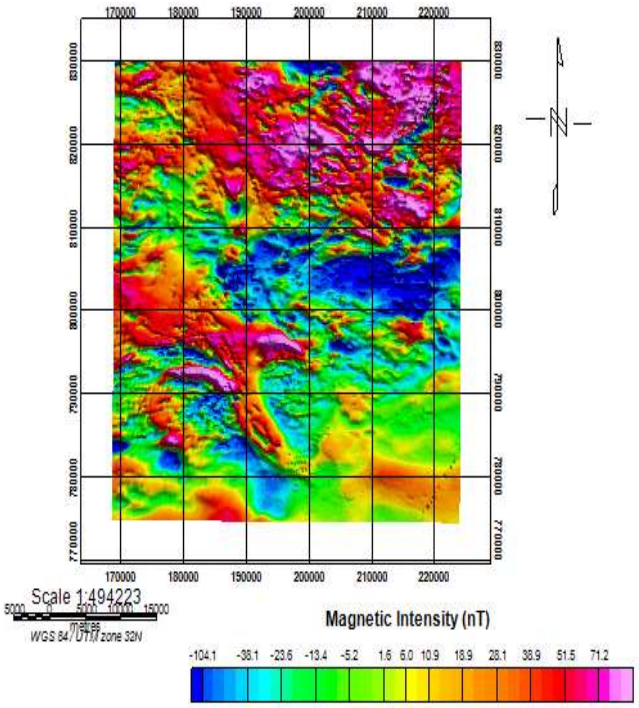

Figure 3. Total magnetic intensity map of the study area

3.2 Residual magnetic anomaly (RMA) map

The residual map created by eliminating the computed regional data (long wavelength anomalies) allows the remaining anomalies to be incorporated into the original airborne magnetic map and displayed. The residual map (Figure 4) demonstrates that the research area is characterized by multiple low-amplitude magnetic intensity anomaly outlines and that the area's tectonic framework is predominantly governed by faulting and fracturing of the rocks. The RMA map (Figure 4) showed mixed regional magnetic zones (F, G, H, I, and J), with the majority of them moving in a NE-SW direction. The placement of magnetic zones was predicated on the distinctive magnetic signature (intensity, shape, texture, and trend). Because the magnetic data were collected at low magnetic latitudes and then decreased to the equator, low magnetic values indicate strong magnetic susceptibility, and high magnetic values indicate low magnetic susceptibility (Balogun 2019). There is a strong magnetic signature zone G in the southern lower section of the image that is cut by a weak magnetic signature zone F. This feature follows a south-to-north axis. The high magnetic sensitivity of body G detected in the lower left part of the RMA image is thought to be attributable to magnetic minerals at the surface, such as crystalline rocks (igneous and metamorphic) with shallow sources (Blanco-Montenegro et al. 2003). The interfering body F in the middle of the G feature is thought to be a sign of an intrusion caused by complicated sources of anomalous bodies that are tightly spaced (Adagunodo et al. 2012). The magnetic response of a lineament network presumed to be fractured with broad southeastern and northeastern trends revealed unstable intensities in the magnetite concentration of the underlying rocks in the studied area. The magnetic values of this feature, which consists of multiple tightly packed anomalous entities with low magnetic signatures in the Southeastern and Northeastern regions of the area (H and J), range from 3.857 to 69.955 nT. According to Bleil and Petersen (1983), locations with high magnetic values are likely to contain crustal limits, deep-seated volcanic rocks, or crystalline igneous or metamorphic rock outcrops. Low magnetic signature regions are thought to have magnetic source rocks near the surface, such as sandstones and river channels.

3.3 Reduction to the equator (RTE)

Although the RTE map (Figure 5) analysis is acceptable for interpreting deep structures, it suffers from background noise caused by wavelengths. The inclination and declination of the earth's magnetic field determine the geometry of the magnetic anomaly in general. To identify the magnetic anomalies that have been identified directly over the magnetic source bodies that caused the anomaly, the RTE filter was applied to the Total Magnetic Intensity (TMI) grid. The TMI grid was reduced to an Equator grid using the Geosoft Oasis Montaj software's Two Dimensional Fast Fourier Transform (2D-FFT) filter. The parameters for the transformation are a -12.10 inclination and a -5.90 declination, which represent the area's mean value. On the RTE magnetic anomaly map, regions with low and high magnetic frequencies reflect places having low and high magnetic imprints, respectively. The total magnetic field anomaly image reduced to the equator displays a nearly symmetrical anomaly, with the E-W striking characteristics (M) clearly delineated at the magnetic equator. The negative anomalies have shifted to the southeast (N), implying that they were caused by the body's well-induced behavior (Owono et al. 2019). A magnetic relief is visible in the study area, but it is disrupted by numerous abnormalities. There are two main magnetic domains in it. High magnetic field values ranging from 49.936 to

106.943 nT characterize the northeastern section. Negative magnetic high point numbers reflect classic anomalous attributes in the low latitude magnetic region, particularly underneath the equator, where the study area is located in Nigeria, with low values ranging between-74.747 nT and -8.627 nT of the magnetic field suggesting areas characterized by geological features such as fracture and fault, with low magnetic components that have the potential to serve as hosts to minerals (Rajaram and Anand 2014; Ozegin and Alile 2021). Hence, the lows in the aforesaid map are associated with magnetic sources. This explained why the data was not reduced to the pole since the research location is in a low latitude zone in which the RTP transformation is unsteady, causing inconsistency in map quality and being occasionally driven by declination-parallel distortions (Blakely 1995; Cooper 1997; Rajaram and Anand 2014).

The magnetic properties of the RMA (Figure 4) and RTE (Figure 5) maps are similar. However, in Eastern Zone H (Figure 4), several RMA patterns are now recognized as linear features going East-West. Other aspects (for example, the high magnetic signature H (Figure 4)) are offset by a low magnetic signature N (Figure 5) that is not visible in the RMA image but visible in the RTE. Several high-value (pinkish) phenomena observed in the RMA image remain high in terms of values (pinkish) in the RTE image, such as the magnetic feature J shown in the northern section of the area (Figures 4 and 5). According to Sunmonu and Alagbe (2014), this section may possibly represent a very shallow basement.

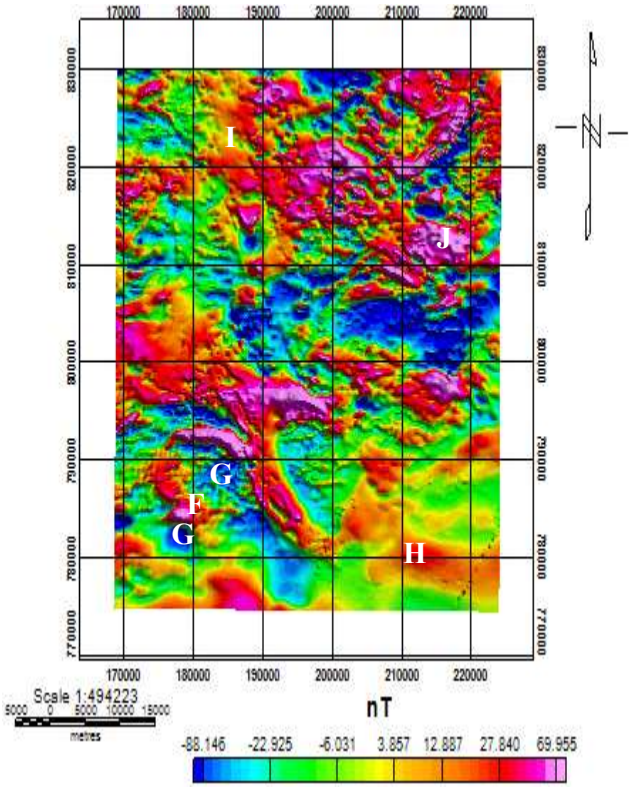

Figure 4. The residual magnetic anomaly map

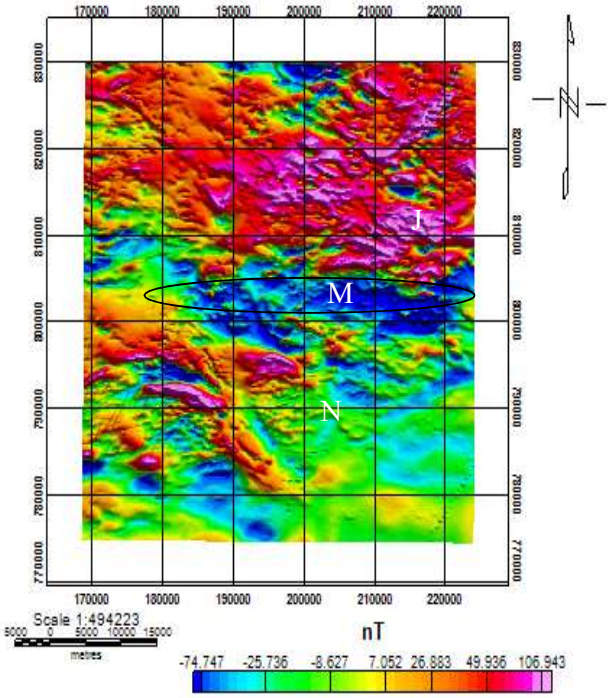

Figure 5. Total magnetic intensity - reduction to the equator (TMI-RTE)

3.4 Vertical derivative (or vertical gradient) map

Figure 6 shows the vertical derivative map, which was applied to total magnetic intensity data to boost the shallow geologic sources of the data and to support the description of the edges of source bodies. This, according to Cooper (1997), also helps to break up the anomalous texture of rocks close to the surface. The anomaly gradient values ranged from −0.084 to 0.031 nT/m. The Oasis Montaj software was used in this study to compute and grid 3D Euler, which resulted in images being generated and the depth of putative magnetic entities being assessed. This highlights a number of rectilinear, subtle features, as well as local and short-wavelength peculiarities. Short-wavelength anomalies on the map are created by small mineralized bodies and/or geological features near the surface (Rajaram and Anand 2014). The ascent of the Precambrian bedrock, which can either be fractured or deformed, is most likely responsible for these geological features or discontinuities. Some of these shear zones are induced by basement tectonics or early Precambrian plate borders (Ngoh et al. 2017). Because of the larger effect of broader regional features in the research area, these anomalies are not visible on the total magnetic map. A probable fault zone has been discovered by anomalies trending NE-SW and NW-SE.

3.5 Total horizontal derivative (THD)

Figure 7 illustrates the total horizontal derivative map. Because the derivative of a quantity is always the largest wherever there is an abrupt shift in its value, extended peak amplitudes on the total horizontal derivative map were utilized to emphasize points exhibiting geological irregularity and hence rectilinear or linear geophysical phenomena.

In the aforesaid figure, it is possible to delimitate two classes of these distinguished features. In the first class, we have moderately short peak amplitudes described with white lines on the map. They are essentially rectilinear geophysical phenomena with NE-SW and E-W trends. It

is found primarily in the Granite gneiss and porphyritic granite regions (designated as "GG" on the THD map) and is clustered around the lithologic contacts AA and BB, which are the Granite gneiss and Quartz-biotite-schist and porphyritic granite and Sandstone, respectively. This indicates a high amount of pressure, as evidenced by extensive deformation around its lithological limits (Balogun 2019). The second type of lineament is the regional scale lineament, which is indicated on the map with black lines and labelled for significant lineaments (or borders). This lineament runs NE-SW and appears to reflect important lithologic contacts and fractured patterns.

3.6 Depth estimate using 3D Euler deconvolution

Figure 8 depicts a basic Euler solution derived from aeromagnetic data with N = 0 which would be adequate for a simple model of a magnetic field induced by the existence of a rock contact as a potential source for the magnetic anomaly detected in the research area. The structural index of zero resulted in a window size of 5 during processing using Oasis Montaj software, equating to a maximum range of 250 m from the source with a 15 percent depth tolerance. Similar to Reid et al. (1990), an Euler map (Figure 8) was created, which shows a large grouping of circles in a logical pattern that identifies the type of potential rock unit contacts. As a result, faults and/or contacts with depth values ranging between < 300 m and > 1000 m are thought to be the cause of such clustering circles. It demonstrates that the majority (± 95%) of the geological or structural features distinctly visible from the color code were discovered within 0–300 m, whereas other features (± 5%) are largely indistinguishable (in terms of color codes).

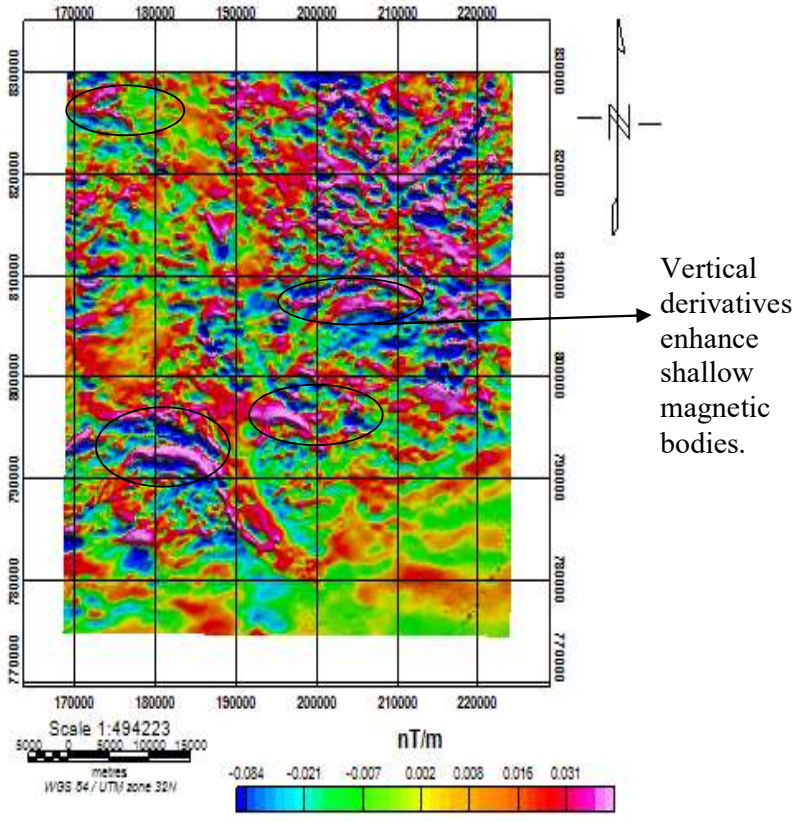

Figure 6. Vertical derivative map of the TMI

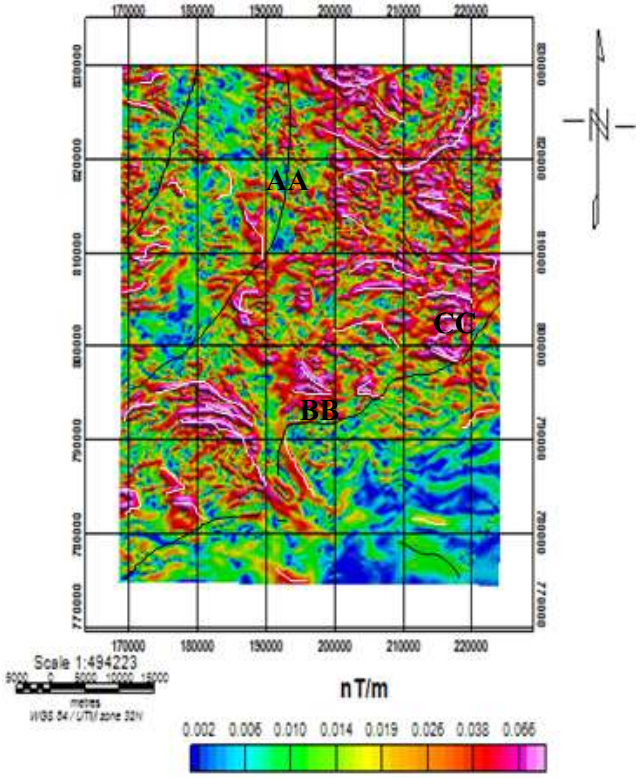

Figure 7. Total horizontal derivative (THD) map of the study area

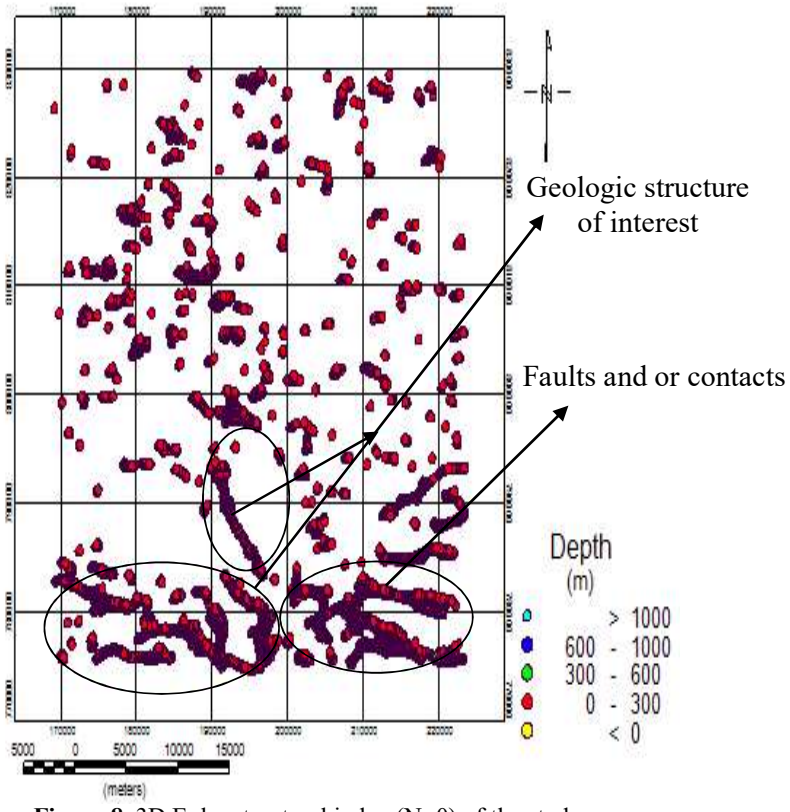

Figure 8. 3D Euler structural index (N=0) of the study area

3.7 Data integration

The results obtained from the airborne magnetic structural maps and 3D Euler deconvolution analysis allowed the generation of an integrated structural map (Figure 9) of the study area. This detailed map showed all structures delineated by the techniques employed. It was created by using single structures (black lines) to represent all the clustered structures in an area. This was done under the assumption that the clustered structures are a result of little discrepancies in locating the same structure by a different approach. The existence of large and small faults, fractures, and rock boundaries was depicted on the map, along with the frequency of fracturing on different rock types in collaboration with a rosette diagram. Accordingly, the rosette diagram (Figure 10**)** of the lineaments primed from the combination of the extracted lineaments shows that there are two major sets of lineaments oriented in the northeast-southwest and ESE-WNW directions, with minor sets oriented in the ENE-WSW and E-W directions. The NE-SW and ESE-WNW trending structures are diagnostic of primary orogeny accompanied by fracturing, thus suggesting comparatively possible potential groundwater exploration and exploitation for solid mineral deposits, and this is consistent with the trend of the continental extension of the oceanic transform faults (Oldenburg and Brune 1975). Rose diagrams were created to aid in the evaluation of structural features and the identification of significant structural trends in the study area.

3.8 Superimposition of extracted lineaments on the geological map

When the geology of the research area is well understood, a comprehensive airborne magnetic map has proven to be very useful (Aero-Service 1984). Lineaments extracted from the airborne magnetic data were circumfused over the geology map (Figure 11) of the study area in an ArcGIS environment. Large concentrations of lineaments were found on sandstone, with a large number of lineaments found on the boundary between the rock types. Sudden trending changes on the vertical derivative map (Figure 6) indicate geological boundaries such as folds and fault zones; they are major weakness zones that influence the near subsurface as well as the basement (Ngoh et al. 2017).

4. Conclusion

The gridded magnetic data was used in this study to establish the geometry and depths of magnetic sources using 3D Euler deconvolution and filtering techniques. The subsurface distributions of regional and local structural deformations are characterized by major faults and some other structural components largely oriented in the NE-SW, ESE-WNW, ENE–WSW, and E–W orientations. Major magnetic lineaments trend in the NE-SW and ESE - WNW directions while the minor magnetic lineaments trend in the ENE– WSW and E–W orientations. The NE-SW and ESE-WNW trending structures are indicative of primary orogeny accompanied by fracturing, and this is in conformity with the trend of the continental extension of the oceanic transform faults. The obtained depths for Euler anomalies ranged from a minimum depth value of 300 to a maximum depth value of >1000 m. The observed structural features delineated are believed to have the potential for groundwater exploration and exploitation of solid mineral deposits.

Acknowledgment

The authors gratefully acknowledge the Nigerian Geological Survey Agency for providing available the Aeromagnetic data used for this research work.

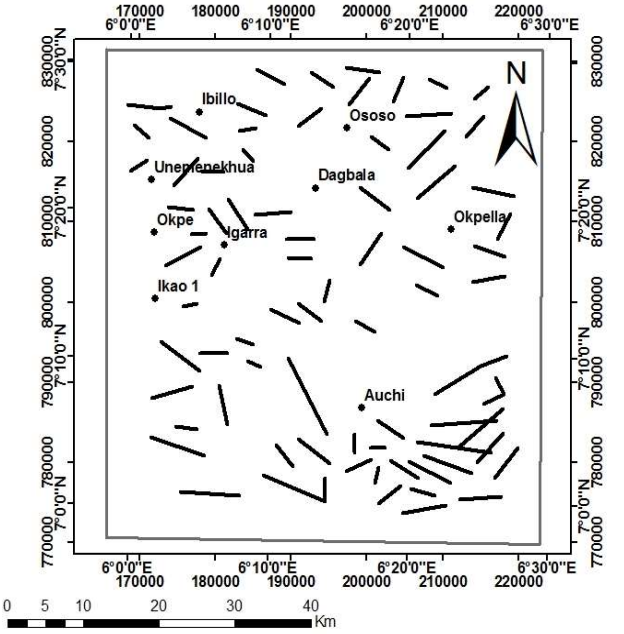

Figure 9. Aeromagnetic lineaments map of the study area

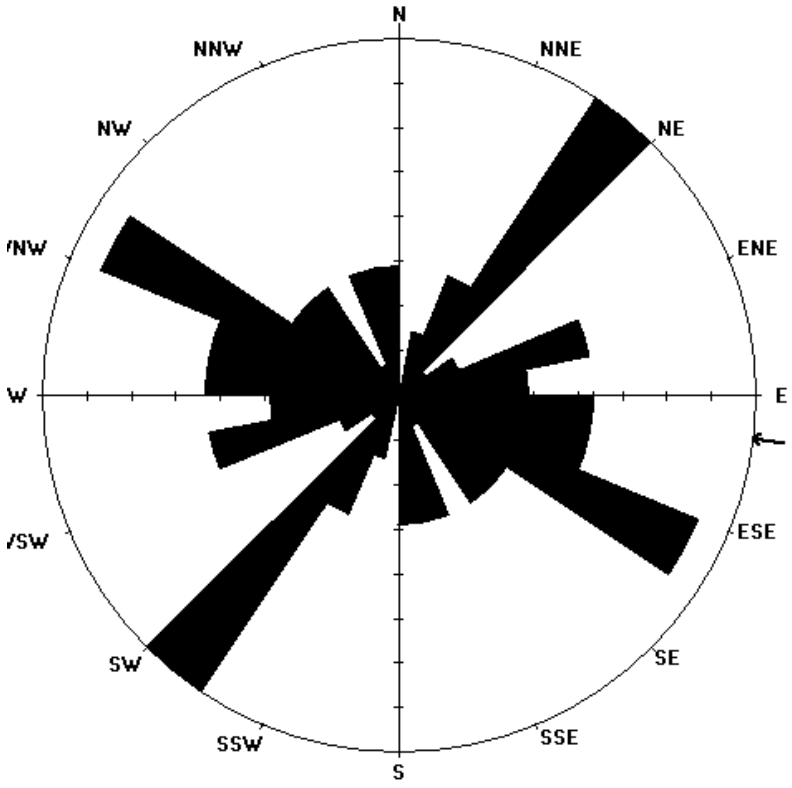

Figure 10. Rose diagram for structural features

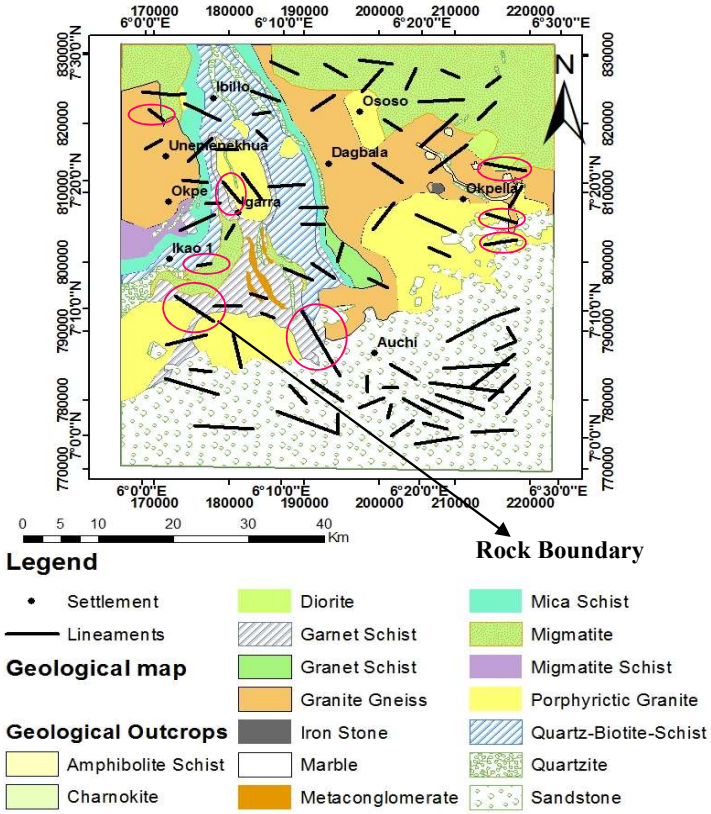

Figure 11. Lineaments on the geologic map of the study area

References

Adagunodo TA, SunmonuLA, Aanuoluwa T, Olafisoye ER, OladejoOP. 2012. Interpretation of ground- magnetic data in Oke-Ogba Area, Akure, Southwestern Nigeria. Advances in Applied Science Research. **3**(5): 3216-3222.

Aero-Service 1984. Final Operational Report of airborne magnetic/ radiation survey in the Eastern Desert, Egypt, Conducted for the Egyptian General Petroleum Corporation, Aero- Service Division, Houston, Western Geophysical Co., Texas, USA.

Anifowose AYB, Bamisaye OA, Odeyemi IB. 2006. Establishing a solid mineral database for part of Southwestern Nigeria. Geospatial World Newsletter. Available: www.geospatialworld.net

Balogun OB. 2019. Tectonic and structural analysis of the Migmatite–Gneiss–Quartzite complex of Ilorin area from aeromagnetic data. NRIAG Journal of Astronomy and Geophysics. **8**(1): 22-33. DOI: 10.1080/20909977.2019.1615795

Blakely RJ. 1995. Potential Theory in Gravity and Magnetic Applications. Cambridge University Press, Australia.

Blanco-Montenegro I, Torta JM, García A, Araña V. 2003. Analysis and modelling of the aeromagnetic anomalies of Gran Canaria (Canary Islands), Earth and Planetary Science Letters. **206**(3-4): 601–616.

Burger RH, Sheehan AF, Jones CH. 2006. Introduction to Applied Geophysics Cambridge University Press, 1-600.

Cooper RJ. 1997. "GravMap and PFproc: Software for Filtering Geophysical Map Data". Computer and Geosciences. **23**(1): 91-101. doi:10.1016/S0098-3004(96)00064-7

Durrheim RJ, Cooper GR J. 1997. Euldep: A Program for the Euler Deconvolution of Magnetic and Gravity Data. Computers and Geosciences. **24**(6): 545-

550.

Florio G, Fedi M, Pasteka R. 2006. On the application of Euler deconvolution to the analytical signal. Geophysics. 71: L87-L93.

Gunn PJ. 1997. Application of aeromagnetic surveys to sedimentary basin studies. AGSO Journal of Australian Geology and Geophysics. **17**(2): 133-144.

Hani A, Nezar H, Mohammed A, Elias S, Abdullah D, Mohammed H, Rida A. 2013. Integration of aeromagnetic data and Landsat imagery for structural analysis purposes: A case study in the southern part of Jordan. Journal of geographic information system. 5: 198-207.

John MU, Emmanuel UE. 2014. Structural analysis using aeromagnetic data: Case study of parts of southern Bida basin, Nigeria and the surrounding basement rocks. Earth Science Research. **3**(2): 27-42.

Moghaddam MM, Sabseparvar M, Mirzaei S, Heydarian N. 2015. Interpretation of Aeromagnetic Data to Locate Buried Faults in North of Zanjan Province, Iran. J Geophys Remote Sensing 4: 143. doi:10.4172/2469-4134.1000143

Mushayandebvu MF, Lesur V, Reid AB, Fairhead JD. 2004. Grid Euler Deconvolution with Constraints for 2D Structures: Geophysics. 69: 489–496. doi:10.1190/1.1707069.

Nabighian MN, Grauch VJ S, Hansen RO, LaFehr TR, Li Y, Peirce JW, Phillips JD, Ruder ME. 2005. The Historical Development of the Magnetic Method in Exploration. Geophysics. 70: (6) 33ND–61ND, 6 FIGS. 10.1190/1.2133784.

Ndougsa-Mbarga T, Feumoe AN, Manguelle-Dicoum E, Fairhead JD. (2012) Aeromagnetic Data Interpretation to Locate Buried Faults in South-East Cameroon. Geophysica. **48**(1-2): 49-63.

Ngoh JD, Mbarga TN, Assemble SP, Meying A, Owono OU. Tabod TC. 2017. Evidence of Structural Facts Inferred from Aeromagnetic Data Analysis over the Guider- Maroua Area (Northern Cameroon). International Journal of Geosciences. 8: 781-800. https://doi.org/10.4236/ijg.2017.86044

Obaje NG. 2009. Geology and mineral resources of Nigeria. Dordrecht. Springer.

Okpoli CC. 2019. High Resolution Magnetic Field Signatures overAkure and Its Environs, Southwestern Nigeria.Earth Sciences Malaysia (ESMY). **3**(1): 09-17 DOI: http://doi.org/10.26480/esmy.01.2019. 09.17

Okpoli CC, Eyitoyo FB. 2016. Aeromagnetic study of Okitipupa region, Southwestern Nigeria. International Basic and Applied Research Journal, **2**(7):1-20.

Okwesili NA, Chiebonam EK, Awucha IE.2019. Euler Deconvolution and Source Parameter Imaging of aeromagnetic data of Guzabure and Gudumbali regions, Chad Basin, North Eastern Nigeria. IOSR Journal of Applied Physics (IOSR-JAP). **11**(3): 1-10.

Olawuyi AK. 2018. Structural Classification Using Aeromagnetic Data And Pseudogravity Transforms: A Case Study Of Pategi Area Of Bida Basin, Nigeria. Tanzania Journal of Science. **44**(3): 192-204.

Oldenburg DW, Brune JN. 1975. An explanation to the orthogonality of ocean ridges and transform faults. Journal of Geophysical Research.82: 803–827.

Owono AOUI, Ndougsa MT, Meying A, Assembe SP, Ngoh JD, Ngoumou PC, Yandjimain J. 2019. Evidence Of Major Structural Features Over The Pan-African Domain In The Bertoua-Mbangue Area (East Cameroon) From A Multiscale Approach Of Modeling And Interpretation Of Aeromagnetic

Data. International Journal of Geophysics. 1-12 Article ID 9148678, https://doi.org/10.1155/2019/9148678

Oyinloye AO. 2011. Geology and geotectonic setting of the basement complex rocks in southwestern Nigeria, Implications on provenance and evolution, earth and environmental sciences. In: Imran A.D. (ed.), In Tech. ISBN: 978-953-307-468-9. Available from http://www.intechopen.com/books/earth-and-environmental-sciences/geology-and geotectonic- setting-of-the-basement-complex-rocks

Ozegin KO, Alile OM. 2021. Depth Estimation Based on Fourier Spectral Analysis of Potential Field Data. Nigerian Research Journal of Engineering and Environmental Sciences **6**(2): 540-547. http://doi.org/10.5281/zenodo.5805122

Paterson NR, Reeves CV. 1985. Applications of gravity and magnetic surveys, the state-of-the-art in 1985. Geophysics. 50: 2558-94.

Peterson JA. 1985. Geology and Petroleum Resources of North-central and Northeastern Africa. U. S. Geological Survey Open-file Report. 54: 85-709.

Phillips JD. 1998. "Processing and Interpretation of Aeromagnetic Data for the Santa Cruz Basin- Patahonia Mountains Area," U.S. Geological Survey Open-File Report 02-98, South-Central Arizona.

Reford MS, Sumner JS. 1964. Aeromagnetics. Geophysics.29:482 – 516.

Reid AB, Allsop JM, Granser H, Millet AJ, Somerton IW. 1990. Magnetic interpretation in three dimensions using Euler deconvolution. Geophysics. 55: 80–91.

Telford WM, Geldart LP, Sheriff RE. 1990. Applied Geophysics (2nd Ed.). Cambridge University Press. 62-135.

Thompson DT. 1982. EULDPH: A new technique for making computer-assisted depth estimates from magnetic data. Geophysics. 47: 31-37.

U.S. Geological Survey. 1997. Open-File Report 95–77 lists many USGS computer programs and databases used to create magnetic maps: http://minerals.er.usgs.gov.